

# A Multi-Load Capacitive Power Relay System With Load-Independent Constant Current Outputs

Ting Chen , Chenwen Cheng , Hong Cheng , Cong Wang , and Chunting Chris Mi , *Fellow, IEEE*

**Abstract**—This article proposes a power relay system to wirelessly power multiple loads via capacitive coupling. The intermediate capacitive relay unit is designed to power the load as well as enhance the power transfer capability, which contains two receiving plates and two transmitting plates. It is proven in this article that the capacitive coupling between the receiving and transmitting plates in the same relay unit can be eliminated by being placed perpendicularly with the help of the proposed split-inductor-based compensation network. A general mathematical model of the multiload capacitive power relay system is established. The  $L$  compensation circuits are employed to compensate the first and the last relays, while the  $LCL$  compensation circuits are designed to compensate the intermediate relays. Thus, the constant current output can be obtained for each load without affecting each other when neglecting the parasitic resistances. Additionally, the load current and efficiency variations versus the load resistance, coupling coefficient, and quality factor are thoroughly analyzed. Finally, a three-load experimental prototype is constructed to verify the feasibility of the proposed multiload capacitive power transfer relay system. The maximum efficiency can reach 86.1% at a power level of 37 W.

**Index Terms**—Capacitive power transfer (CPT), constant current (CC) outputs, multiple loads, power relay.

## I. INTRODUCTION

CAPACITIVE power transfer (CPT) utilizes an electric field to transfer energy from the transmitter to the receiver. Recently, CPT has received extensive attention from researchers because of its desirable characteristics of no sensitivity to surrounding metal objects and no thermal effects generated by the eddy current [1], [2]. To enhance the power transfer capability and achieve output stability, various compensation topologies such as  $LCL-L$  [3],  $LC-LC$  [4], [5],  $LCL-LCL$  [6],  $LCLC-LCLC$  [7], [8], etc. have been proposed.

Manuscript received July 14, 2021; revised September 24, 2021; accepted October 19, 2021. Date of publication October 27, 2021; date of current version January 19, 2022. This work was supported in part by the Fundamental Research Funds for the Central Universities, in part by the Fujian Key Laboratory of New Energy Generation and Power Conversion under Grant KLIF-202101, and in part by the Scholarship from China Scholarship Council. Recommended for publication by Associate Editor S. Williamson. (*Corresponding author: Chenwen Cheng.*)

Ting Chen, Hong Cheng, and Cong Wang are with the China University of Mining and Technology, Beijing 100083, China (e-mail: mia\_tingchen@outlook.com; chengh@cumtb.edu.cn; wangc@cumtb.edu.cn).

Chenwen Cheng is with Southeast University, Nanjing 210096, China (e-mail: cheng.cwen@gmail.com).

Chunting Chris Mi is with San Diego State University, San Diego, CA 92182 USA (e-mail: mi@ieee.org).

Color versions of one or more figures in this article are available at <https://doi.org/10.1109/TPEL.2021.3123542>.

Digital Object Identifier 10.1109/TPEL.2021.3123542

Most of the published CPT technology can only power one load [9], [10]. In some cases, however, multiple loads need to be powered simultaneously with a constant current (CC), such as charging batteries in series [11] and powering multiple light-emitting diodes [12]. Su *et al.* [13] adopted a mixed high-order resonant topology consisting of a  $\Pi$ - $CLC$  resonant network in the transmitter and multiple  $T$ - $CLC$  resonant networks in the receivers. In this article, large transmitting plates are required to provide enough capacitive coupling to all receiving plates. However, the capacitive coupling model in [13] was not accurate since each transmitter–receiver pair was simply modeled as two capacitances and some parasitic capacitances were neglected. In [14], two shunt inductors are connected in parallel with the capacitive coupler at the primary side and the secondary side, respectively, to achieve maximum power transfer. Nevertheless, the receivers are then coupled with each other, which induces mutual interference between loads and increases system control complexity. In [15], the  $LCCL$  primary compensation circuit is adopted to ensure a load-independent voltage across two transmitting plates of the capacitive coupler, while multiple parallel-series  $LC$  secondary compensation circuits are employed for all the receivers to achieve CC outputs. Although the capacitive coupler in each transmitter–receiver pair is modeled as an equivalent  $\Pi$ -type model when considering all six coupling capacitances, the receivers are required to be placed very far from each other in order to neglect the cross-coupling among them. In addition to the aforementioned single-input and multioutput CPT system, Vu *et al.* [16] and Kumar *et al.* [17] proposed a multi-input and multioutput CPT system which was deployed by multiple single-input and single-output CPT systems in parallel. Nevertheless, cross-coupling capacitances between two arbitrary plates in the transmitter and receiver respectively were not taken into account in [16]. Although Kumar *et al.* [17] adopted tuning inductors to compensate the capacitive cross-coupling capacitance between two adjacent transmitters and receivers, respectively, it is difficult to obtain the compensation inductances accurately because the high-frequency CPT system is sensitive to parameter deviations. In the above-mentioned structures, a large separation space between adjacent transmitters or receivers is essential to minimize the cross-coupling among them. Furthermore, the transfer distance between the coupled transmitter and receiver is limited to ensure a large mutual capacitance.

Recently, a novel power relay structure was proposed for the inductive power transfer (IPT) system in [18] and [19], where two relay coils were grouped into one relay unit and the receiving

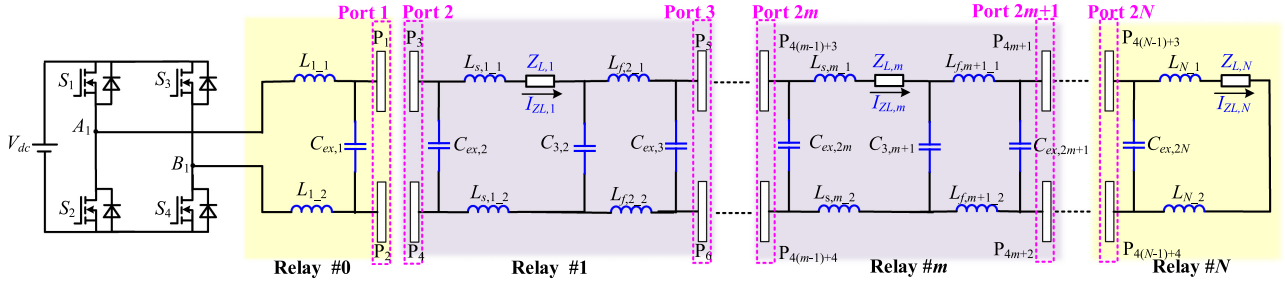


Fig. 1. Topology of the proposed multiload CPT relay system.

relay coil was placed perpendicularly to the transmitting relay coil to achieve magnetic decoupling. With the *CLC* compensation network in [18] and the *LCC* compensation network in [19], CC outputs can be obtained. This power relay structure provides a different solution for the multiple wireless power transfer system. Zhang *et al.* [20] proposed a CPT power relay system where a relay is placed between the transmitter and the receiver to extend the power transfer distance, and *LC* compensation networks are adopted to compensate the capacitive coupling interface. However, only one load can be powered in [20]. Up until now, no paper has investigated the CPT power relay system for powering multiple loads simultaneously.

As a counterpart of the multiload IPT power relay system in [18], this article proposes a novel multiload CPT relay system, where each intermediate power relay consists of two receiving plates and two transmitting plates placed perpendicularly to each other. With the help of the split-inductor-based compensation network, each relay can achieve load power decoupling. Moreover, a general mathematical model of the multiple capacitive coupling interface considering all coupling capacitances is presented. Compared with the modeling method in [21], no complicated matrix operations are required and the compensation network is taken into account during the modeling process. In addition, the *L* compensation network is designed in the first and last relay, and the *LCL* compensation network is designed in the intermediate relay to achieve load-independent CC outputs. The effect of parasitic resistances on the load output currents and system efficiency are also elaborated. An experimental prototype with three loads is established to demonstrate the validity of the proposed multiload CPT relay system.

The contributions of this article are summarized as follows.

- 1) A multiload CPT system using a capacitive power relay to transfer energy is proposed.
- 2) A novel capacitive power relay structure is designed where the two receiving plates are perpendicular to the transmitting plates. Together with the proposed split-inductor compensation network, the coupling between the receiving and transmitting pads can be neglected, which greatly simplifies the systems design and analysis.
- 3) A general mathematical model of the capacitive coupling interface with *L* and *LCL* compensation network is established so that multiple load-independent CC outputs can be achieved.

## II. SCHEMATIC OF THE PROPOSED MULTILOAD CPT RELAY SYSTEM

### A. System Description

The proposed multiload CPT relay system with multiple CC outputs is shown in Fig. 1, which consists of an inverter and  $(N+1)$  capacitive power relays. The dc-link voltage of the inverter is  $V_{dc}$  and the inverter operates in a complementary manner. The fundamental component of the inverter output voltage  $v_{in1}$  can be calculated as

$$v_{in1} = V_{in1} \sin(\omega_0 t) = \left(2\sqrt{2}V_{dc}/\pi\right) \sin(\omega_0 t) \quad (1)$$

where  $V_{in1}$  is the rms value of the fundamental component of the inverter output voltage and  $\omega_0$  is the operational angular frequency of the system. Relay #0 contains two plates  $P_1$  and  $P_2$ , which transfers power to relay #1. Relay # $m$  ( $m = 1, 2, \dots, N-1$ ) contains four plates, where plates  $P_{4(m-1)+3}$  and  $P_{4(m-1)+4}$  are used to receive power from the previous relay, while plates  $P_{4m+1}$  and  $P_{4m+2}$  are used to transfer power to the next one. Relay # $N$  contains two plates  $P_{4(N-1)+3}$  and  $P_{4(N-1)+4}$ , and receives power from Relay # $N-1$ . At each receiving end, usually the load circuit should contain a full-bridge rectifier to transform the ac power to a dc source for the real load. The full-bridge rectifier with a real load can be modeled as a load impedance  $Z_{L,m}$  ( $m = 1, 2, \dots, N$ ).  $L_{L,1}$  and  $L_{L,2}$  are the compensation inductances in Relay #0.  $L_{L,N,1}$  and  $L_{L,N,2}$  are the compensation inductances in relay # $N$ .  $L_{s,m-1}$ ,  $L_{s,m-2}$ ,  $L_{f,m+1-1}$ ,  $L_{f,m+1-2}$  and  $C_{3,m}$  are the compensation inductances and compensation capacitance in relay # $m$  ( $m = 1, 2, \dots, N-1$ ).  $P_{4(m-1)+1}$  and  $P_{4(m-1)+2}$  form port  $2m-1$ , while  $P_{4(m-1)+3}$  and  $P_{4(m-1)+4}$  form port  $2m$  ( $m = 1, 2, \dots, N$ ). External capacitors  $C_{ex,2m-1}$  ( $m = 1, 2, \dots, N$ ) and  $C_{ex,2m}$  ( $m = 1, 2, \dots, N$ ) are connected in parallel with port  $2m-1$  and port  $2m$ , respectively.

Fig. 2 shows the capacitive coupling interface of the proposed CPT power relay system. In relay # $m$  ( $m = 1, 2, \dots, N-1$ ), the receiving plates are designed to be perpendicular to the transmitting plates. The aluminum oxide ceramic is embedded between every two adjacent relays to enhance the capacitive coupling. The dimensions of the copper plates and the ceramic plates are  $l_1 * l_2 * d_2$  and  $l_1 * (d_1 + 2l_2) * d_3$ , respectively, where  $l_1$  and  $l_2$  are the length and width of all copper plates and ceramic plates;  $d_1$  is the separation distance between two adjacent copper

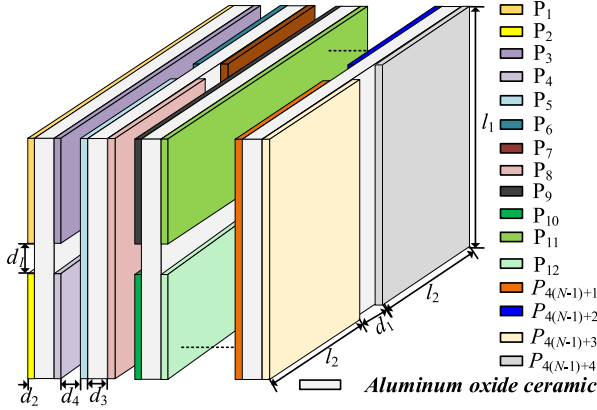


Fig. 2. Capacitive coupler of the proposed CPT power relay system.

plates;  $d_2$  is the height of all copper plates;  $d_3$  and  $d_4$  are the heights of the ceramic and air-gap. In addition,  $l_1 = d_1 + 2l_2$ .

### B. Decoupling Method and Modeling

The coupling capacitance between any two plates  $P_i$  and  $P_j$  is defined as  $C_{i,j}$  ( $i, j = 1, 2, \dots, 4(N-1)+4$ ,  $i \neq j$ ), totaling to  $C_{4N}^2$  coupling capacitances. The complicated electric coupling inevitably increases difficulties in the systems design and analysis. In order to achieve decoupling in each relay unit in Fig. 1, as well as the elimination of undesired mutual capacitance, the split-inductor-based compensation networks are employed. This connotes that the above inductances in the forward path should be equal to the inductances in the return path, i.e.,  $L_{1-1} = L_{1-2}$ ,  $L_{N-1} = L_{N-2}$ ,  $L_{s,m-1} = L_{s,m-2}$  ( $m = 1, 2, \dots, N-1$ ), and  $L_{f,m-1} = L_{f,m-2}$  ( $m = 2, 3, \dots, N$ ). The reasons are analyzed in detail as follows.

First, it is assumed  $Z_{L,1} = Z_{L,2} = \dots = Z_{L,N} = 0$ . The influence of load impedances will be discussed in Section II-D. As shown in Fig. 1, the proposed relay structure has  $2N$  ports. Without losing the general characteristics, the following analysis will take the simplest two-load CPT system with one intermediate power relay as an example to facilitate the analysis. The coupling capacitance mode is shown in Fig. 3. The inverter's output voltage can be modeled as two sinusoidal voltage sources  $v_{s1} = 0.5V_{in1}\sin(\omega_0 t)$  and  $v_{s2} = 0.5V_{in1}\sin(\omega_0 t + \pi)$  applied at nodes A and B, respectively, which has the same magnitude but  $180^\circ$  phase difference. Similarly, the second load voltage  $v_{ZL,2}$  can be modeled as two sinusoidal voltage sources  $v_{s3}$

$= 0.5V_{ZL,2}\sin(\omega_0 t + \varphi)$  and  $v_{s4} = 0.5V_{ZL,2}\sin(\omega_0 t + \varphi + \pi)$  applied at nodes C and D, where  $V_{ZL,2}$  is the rms value of the second load voltage and  $\varphi$  is the initial phase angle of  $v_{ZL,2}$ . When  $v_{s1}$ ,  $v_{s2}$ ,  $v_{s3}$ , and  $v_{s4}$  work together, the current flowing through  $C_{i,j}$  ( $i, j = 1, 2, \dots, 8$ ,  $i \neq j$ ) is defined as  $i_{C_{i,j}}$  and the direction is marked in Fig. 3(a). When  $v_{sl}$  ( $l = 1, 2, 3, 4$ ) is applied while others are short-circuited, the current flowing through  $C_{i,j}$  ( $i, j = 1, 2, \dots, 8$ ,  $i \neq j$ ) is defined as  $i_{C_{i,j}l}$ . The coupling capacitances at the symmetrical position have the same values because the facing area between two copper plates are the same as shown in Fig. 2. On the inverter side, as shown in Fig. 3(b) and (c),  $v_{s1}$  and  $v_{s2}$  are applied respectively while other voltage sources are short-circuited. It can be derived that the corresponding currents flowing through coupling capacitances located at the symmetrical position have the same amplitude but opposite directions because the circuit is symmetrical when split-inductors are used, i.e.,  $i_{C1,7-1} = -i_{C2,8-2}$ ,  $i_{C1,8-1} = -i_{C2,7-2}$ ,  $i_{C1,5-1} = -i_{C2,6-2}$ ,  $i_{C1,6-1} = -i_{C2,5-2}$ ,  $i_{C3,7-1} = -i_{C4,8-2}$ ,  $i_{C3,8-1} = -i_{C4,7-2}$ ,  $i_{C3,5-1} = -i_{C4,6-2}$ ,  $i_{C3,6-1} = -i_{C4,5-2}$ , ...,  $i_{C2,7-1} = -i_{C1,8-2}$ , and  $i_{C2,8-1} = -i_{C1,7-2}$ . Similarly, when  $v_{s3}$  or  $v_{s4}$  works while others are short-circuited, as shown in Fig. 3(d) and (e), the above conclusion is still tenable. So, it can be noted that  $i_{C1,7-3} = -i_{C2,8-4}$ ,  $i_{C1,8-3} = -i_{C2,7-4}$ ,  $i_{C1,5-3} = -i_{C2,6-4}$ ,  $i_{C1,6-3} = -i_{C2,5-4}$ ,  $i_{C3,7-3} = -i_{C4,8-4}$ ,  $i_{C3,8-3} = -i_{C4,7-4}$ ,  $i_{C3,5-3} = -i_{C4,6-4}$ ,  $i_{C3,6-3} = -i_{C4,5-4}$ , ...,  $i_{C2,7-3} = -i_{C1,8-4}$ , and  $i_{C2,8-3} = -i_{C1,7-4}$ . Applying the principle of superposition, the currents flowing through all coupling capacitances in Fig. 3(a) are equal to the sum of currents when four independent sources work separately. Then applying Kirchhoff's current law at nodes  $P_1, P_2, P_3, P_4, P_5, P_6, P_7$ , and  $P_8$ , respectively, the following equation can be obtained:

$$\begin{cases} i_{C1,7} + i_{C1,8} = -(i_{C2,7} + i_{C2,8}), & i_{C1,7} + i_{C2,7} \\ & = -(i_{C1,8} + i_{C2,8}) \\ i_{C1,5} + i_{C1,6} = -(i_{C2,5} + i_{C2,6}), & i_{C1,5} + i_{C2,5} \\ & = -(i_{C1,6} + i_{C2,6}) \\ i_{C3,7} + i_{C3,8} = -(i_{C4,7} + i_{C4,8}), & i_{C3,7} + i_{C4,7} \\ & = -(i_{C3,8} + i_{C4,8}) \\ i_{C3,5} + i_{C3,6} = -(i_{C4,5} + i_{C4,6}), & i_{C3,5} + i_{C4,5} \\ & = -(i_{C3,6} + i_{C4,6}) \\ & i_{a1} = -i_{a2}, i_{b1} = -i_{b2}, i_{c1} = -i_{c2}, i_{d1} = -i_{d2} \end{cases} \quad (2)$$

where  $i_{a1}$ ,  $i_{a2}$ ,  $i_{b1}$ ,  $i_{b2}$ ,  $i_{c1}$ ,  $i_{c2}$ ,  $i_{d1}$ , and  $i_{d2}$  are defined in Fig. 3(a). Thus, it can be identified from (2) that all coupling

$$C_{\text{port},a} = \begin{cases} C_{1,2} + \sum_{\substack{x=3,5,7,\dots,4(N-1)+3 \\ y=4,6,8,\dots,4(N-1)+4}} \frac{(C_{1,x}+C_{1,y}) \cdot (C_{2,x}+C_{2,y})}{C_{1,x}+C_{1,y}+C_{2,x}+C_{2,y}} & a = 1 \\ C_{i,j} + \sum_{\substack{x=1,3,5,\dots,i-2 \\ y=2,4,6,\dots,j-2}} \frac{(C_{x,i}+C_{y,i}) \cdot (C_{j,x}+C_{j,y})}{C_{x,i}+C_{y,i}+C_{j,x}+C_{j,y}} + \sum_{\substack{x=i+2,i+4,\dots,4(N-1)+3 \\ y=j+2,j+4,\dots,4(N-1)+4}} \frac{(C_{i,x}+C_{i,y}) \cdot (C_{j,x}+C_{j,y})}{C_{i,x}+C_{i,y}+C_{j,x}+C_{j,y}} & a = 2, 3, \dots, 2N-1 \\ i \neq j; i = 3, 5, 7, 9, \dots, 4(N-1)+1; j = 4, 6, 8, 10, \dots, 4(N-1)+2; a = j/2 \\ C_{4(N-1)+3,4(N-1)+4} + \sum_{\substack{x=1,3,5,\dots,4(N-1)+1 \\ y=2,4,6,\dots,4(N-1)+2}} \frac{(C_{x,4(N-1)+3}+C_{y,4(N-1)+3}) \cdot (C_{x,4(N-1)+4}+C_{y,4(N-1)+4})}{C_{x,4(N-1)+3}+C_{y,4(N-1)+3}+C_{x,4(N-1)+4}+C_{y,4(N-1)+4}} & a = 2N \end{cases} \quad (3)$$

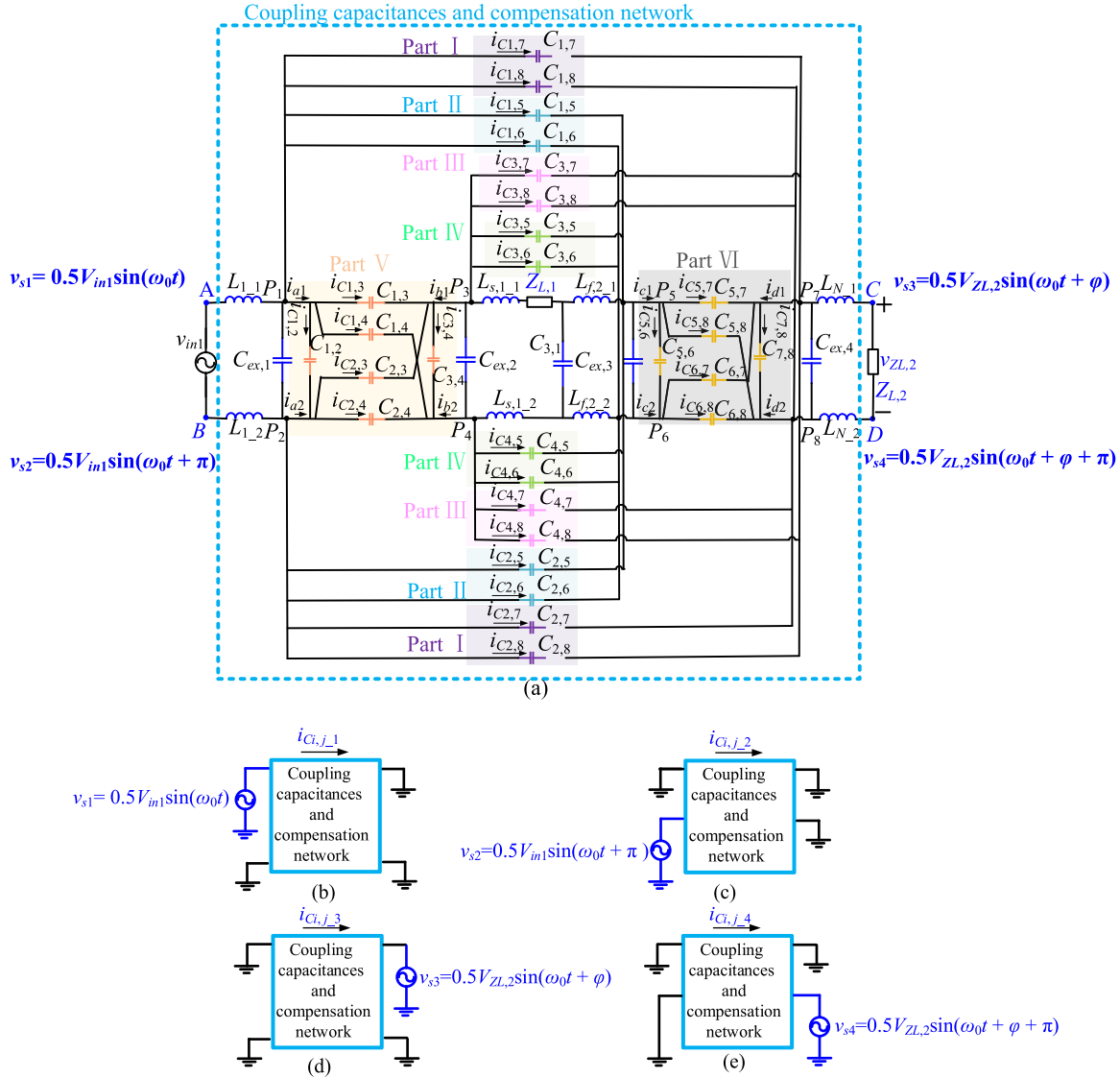


Fig. 3. Coupling capacitance model of the simplest multiload CPT system with one intermediate power relay. (a)  $v_{s1}$ ,  $v_{s2}$ ,  $v_{s3}$ , and  $v_{s4}$  works together. (b) Only  $v_{s1}$  works and other power supplies are short-circuited. (c) Only  $v_{s2}$  works and other power supplies are short-circuited. (d) Only  $v_{s3}$  works and other power supplies are short-circuited. (e) Only  $v_{s4}$  works and other power supplies are short-circuited.

capacitances in the power relay structure consisting of one intermediate relay can be regarded as six two-port networks, i.e., parts I–VI, as shown in Fig. 3(a). The above analysis process and conclusion can be extended to the system with  $N$  loads which is a  $2N$ -port network. The currents flowing through the coupling capacitances located at the symmetrical position are still equal to that of the proposed relay structure and split-inductors. Thus, all coupling capacitances in the proposed  $2N$ -port relay structure can be divided into  $C_{2N}^2$  two-port networks. Then, the two-port network analysis method in [6] can be used to calculate the self-capacitances and mutual capacitance. The self-capacitance of port  $a$  is defined as  $C_{\text{port}, a}$  ( $a = 1, 2, \dots, 2N$ ) and is the sum of the self-capacitance of all two-port networks containing port  $a$ , which can be calculated as (3) shown at bottom of the previous page.

The mutual capacitance  $C_{Ma, b}$  ( $a, b = 1, 2, \dots, 2N, a \neq b$ ) between port  $a$  and port  $b$ , which were formed by plates  $P_{2a-1}$ ,

$P_{2a}$ ,  $P_{2b-1}$ , and  $P_{2b}$ , can be derived as

$$C_{Ma, b} = \frac{C_{2a, 2b} \cdot C_{2a-1, 2b-1} - C_{2a-1, 2b} \cdot C_{2a, 2b-1}}{C_{2a, 2b} + C_{2a-1, 2b-1} + C_{2a-1, 2b} + C_{2a, 2b-1}}. \quad (4)$$

The sum of mutual capacitances between port  $a$  and the other ports are defined as  $C_{M\text{port}, a}$  ( $a = 1, 2, \dots, 2N$ ), which can be calculated as

$$C_{M\text{port}, a} = \sum_{b=1}^{2N} C_{Ma, b} \quad (b \neq a). \quad (5)$$

Thus, the equivalent II model of the proposed relay structure is shown in Fig. 4.  $V_1, I_1, V_2, I_2, \dots, V_{2N}, I_{2N}$  are the terminal voltages and currents of the  $2N$  ports.

It should be noted that in relay  $\#m$  ( $m = 1, 2, \dots, N-1$ ) that is formed by port  $2m$  and port  $2m+1$ ,  $C_{4(m-1)+3, 4m+1} = C_{4(m-1)+3, 4m+2} = C_{4(m-1)+4, 4m+1} = C_{4(m-1)+4, 4m+2}$  can be derived because of the symmetrical capacitive coupling



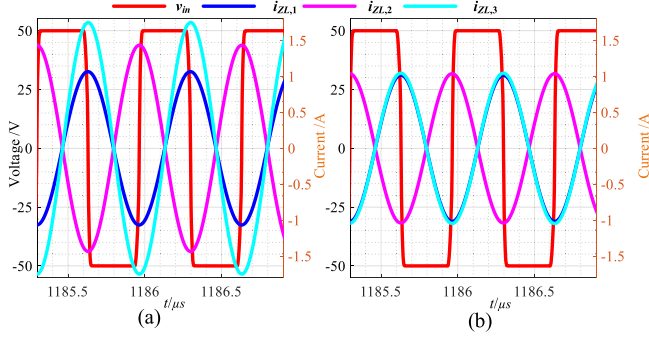


Fig. 7. Simulation results. (a) Without split inductors. (b) With split inductors. ( $Z_L = 0$ ).

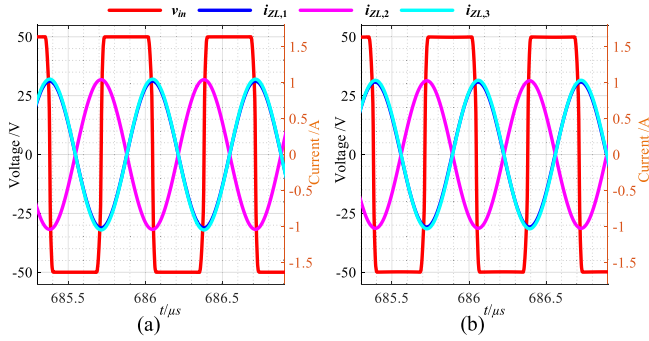


Fig. 8. Simulation results with different load impedance under the premise of split inductors. (a)  $Z_L = 20 - j150$ . (b)  $Z_L = 500 - j600$ .

that the load resistances have a negligible effect on the system decoupling performance and outputs.

### III. SYSTEM ANALYSIS

#### A. CC Output

In order to facilitate the analysis, the parasitic resistances of the compensation circuit are not considered first because their values are usually small. The influence of the parasitic resistances on the system outputs and efficiency will be analyzed in the following section. Based on the above modeling of the capacitive coupler interface and the band-pass filter characteristic of the resonant circuits, the equivalent  $\Pi$  model of the proposed multiload power relay system in Fig. 1 using the fundamental harmonic approximation (FHA) method can be redrawn as in Fig. 9. Since the currents flowing through the split inductors in the forward path and the return path are identical, the two split inductors can be combined as one inductor during the analysis, i.e.,  $L_1 = L_{1,1} + L_{1,2}$ ,  $L_N = L_{N,1} + L_{N,2}$ ,  $L_{s,m} = L_{s,m-1} + L_{s,m,2}$  ( $m = 1, 2, \dots, N-1$ ), and  $L_{f,m} = L_{f,m-1} + L_{f,m,2}$  ( $m = 2, 3, \dots, N$ ).  $C_{s,2m-1}$  and  $C_{s,2m}$  are the self-capacitances in the  $m$ th transmitter and receiver, respectively, which can be calculated as

$$\begin{aligned} C_{s,2m-1} &= C_{\text{port},2m-1} + C_{\text{ex},2m-1} \\ C_{s,2m} &= C_{\text{port},2m} + C_{\text{ex},2m} \end{aligned} \quad (6)$$

where  $C_{\text{port},2m-1}$  and  $C_{\text{port},2m}$  are the internal self-capacitances of port  $2m-1$  and port  $2m$  in the  $m$ th transmitter–receiver pair, respectively, which can be obtained from (3). The mutual capacitances between port  $2m-1$  and port  $2m$  can be obtained from (4) and are redefined as  $C_{M,m}$  ( $m = 1, 2, \dots, N$ ). Accordingly, the coupling coefficient  $k_{c,m}$  ( $m = 1, 2, \dots, N$ ) among them can be derived as

$$k_{c,m} = C_{M,m} / \sqrt{C_{s,2m-1} C_{s,2m}}. \quad (7)$$

In order to facilitate the derivation of resonant conditions to obtain CC outputs and realization of zero phase angle of the input impedance, inductance  $L_{s,m}$  can be regarded as two inductances  $L_{sx,m}$  and  $L_{sy,m}$  connected in series. Inductance  $L_{f,m}$  can also be regarded as two inductances  $L_{fx,m}$  and  $L_{fy,m}$  connected in series. As can be seen from Figs. 1 and 9, the proposed multiload CPT power relay system can be regarded as  $N$  transmitter–receiver pair in cascade. The  $m$ th ( $m = 1, 2, \dots, N$ ) transmitter–receiver pair consisting of  $L_{sx,m}$ ,  $L_{sy,m}$ ,  $L_{fx,m}$  and  $L_{fy,m}$  is redrawn in Fig. 10. It should be noted that  $C_{3,m}$  and  $L_{fx,m}$  do not exist in the first transmitter–receiver pair, and  $L_{sy,N}$  does not exist in the  $N$ th transmitter–receiver pair.

$I_{ZL,m}$  ( $m = 1, 2, \dots, N$ ) is the output current of the  $m$ th transmitter–receiver pair and is also the input current of the subsequent transmitter–receiver pair. Provided that the following resonant condition is met:

$$\omega_0^2 = 1 / (L_{sy,m-1} C_{3,m}) = 1 / (L_{fx,m} C_{3,m}). \quad (8)$$

A constant voltage source  $V_{AmBm}$  ( $m = 2, 3, \dots, N$ ) can be obtained as shown in

$$V_{AmBm} = I_{RL,m-1} / (j\omega_0 C_{3,m}) \quad (9)$$

where  $C_{\text{pri},m}$  is the equivalent input capacitance seen from the primary side and can be calculated as [6]

$$C_{\text{pri},m} = C_{s,2m-1} - C_{M,m}^2 / C_{s,2m}. \quad (10)$$

Provided that the following resonant condition is met:

$$\omega_0^2 = 1 / (L_{fy,m} C_{\text{pri},m}) = 1 / (L_{sx,m} C_{\text{pri},m}). \quad (11)$$

A CC output  $I_{ZL,m}$  ( $m = 1, 2, \dots, N$ ) can be obtained using Norton's Theorem, which can be derived as

$$\begin{aligned} I_{ZL,m} &= \frac{j\omega_0 C_{M,m} V_{AmBm}}{1 - \omega_0^2 L_{fy,m} C_{s,2m-1}} \\ &= -\frac{C_{M,m} I_{ZL,m-1}}{C_{3,m}} \left( \frac{1}{k_{c,m}^2} - 1 \right) \end{aligned} \quad (12)$$

where  $V_{A1B1}$  is equal to  $V_{in1}$ ,  $L_{fy,1}$  is equal to  $L_1$ , and  $L_{sx,N}$  is equal to  $L_2$ . According to (9) and (12), the first load output current lags the inverter output voltage by  $90^\circ$ . The load output current phase angle difference between adjacent transmitter–receiver pairs is  $180^\circ$ . To ensure equal load current outputs, the input and output currents of each transmitter–receiver pair are required to be identical. Substituting (9) into (12),  $C_{3,m}$  ( $m = 1, 2, \dots, N$ ) should satisfy the following condition:

$$C_{3,m} = -C_{M,m} (1/k_{c,m}^2 - 1). \quad (13)$$

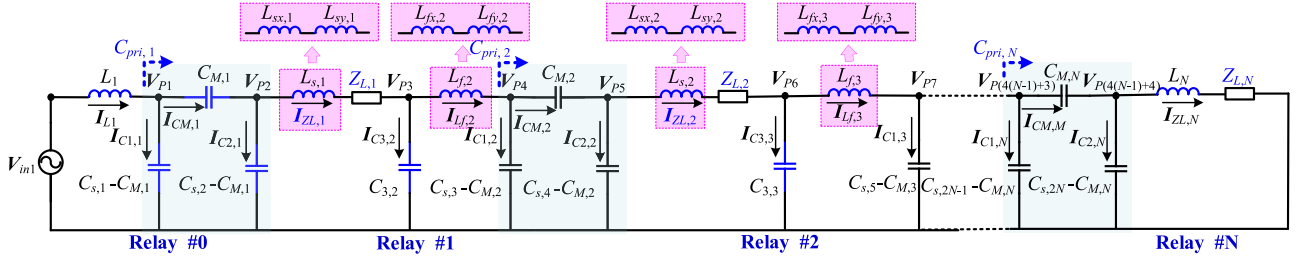


Fig. 9. Equivalent II model of the proposed multiloop CPT relay system using the FHA method.

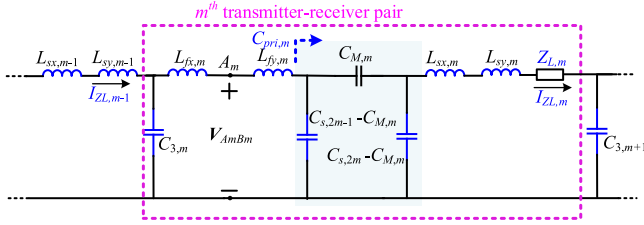


Fig. 10. Equivalent II model of the  $m$ th transmitter-receiver pair of the proposed multiloop CPT relay system.

Since  $L_{s,m} = L_{sx,m} + L_{sy,m}$ , and  $L_{f,m} = L_{fx,m} + L_{fy,m}$ , the resonant conditions consisting of  $L_1$ ,  $L_{s,m}$ ,  $L_{f,m}$ , and  $L_N$  in Fig. 9 can be obtained and summarized as in (14) according to (8) and (11)

$$\begin{aligned} \omega_0^2 &= \frac{1}{L_1 C_{pri,1}} = \frac{1}{L_{s,m} C_{pri,m}} + \frac{1}{L_{s,m} C_{3,m+1}} \\ &= \frac{1}{L_{f,m} C_{3,m}} + \frac{1}{L_{f,m} C_{pri,m}} = \frac{1}{L_N C_{pri,N}}. \end{aligned} \quad (14)$$

In this case, once the capacitive coupler in the multiloop CPT relay system is determined beforehand,  $C_M$ ,  $m$ ,  $C_{s,2m-1}$ , and  $C_{s,2m}$  are known. Then  $L_1$ ,  $L_N$ ,  $L_{s,m}$  ( $m = 1, 2, \dots, N-1$ ) and  $L_{f,m}$  ( $m = 2, 3, \dots, N$ ) can be obtained from (10), (13), and (14).

Since the capacitive coupling interface of each relay has the same structure, the mutual capacitances between each transmitter-receiver pair are identical, which satisfies  $C_{M,1} = C_{M,2} = \dots = C_{M,N} = C_M$ . When the self-capacitances of each transmitter-receiver are identical, i.e.,  $C_{s,1} = C_{s,3} = \dots = C_{s,2N-1} = C_1$ , and  $C_{s,2} = C_{s,4} = \dots = C_{s,2N} = C_2$ , the coupling coefficients of each transmitter-receiver are identical, which means  $k_{c,1} = k_{c,2} = \dots = k_{c,N} = k$ . Substituting the above equations into (10), (13), and (14), the compensation inductances and compensation capacitance at the same position in each transmitter-receiver are also identical, i.e.,  $L_{s,1} = L_{s,2} = \dots = L_{s,N-1} = L_{s,N}$ ,  $L_{f,2} = L_{f,3} = \dots = L_{f,N} = L_{f,N}$ ,  $C_{3,2} = C_{3,3} = \dots = C_{3,N} = C_3$ . Moreover, if all load impedances are the same, i.e.,  $Z_{L,1} = Z_{L,2} = \dots = Z_{L,N}$ , all loads can acquire identical load power.

### B. Power Transfer Capability

In a practical system, parasitic resistance is inherent and will affect the load current output characteristic and system efficiency. In Fig. 9, the quality factor of  $L_1$ ,  $L_s$ ,  $L_f$ ,  $L_N$ ,  $C_3$ ,  $C_M$ ,

$C_1-C_M$ , and  $C_2-C_M$  is defined as  $Q_{L1}$ ,  $Q_{Ls}$ ,  $Q_{Lf}$ ,  $Q_{LN}$ ,  $Q_{C3}$ ,  $Q_{CM}$ ,  $Q_{C1}$ , and  $Q_{C2}$ , respectively. The parasitic resistances and admittances of all components can be expressed as

$$\left\{ \begin{aligned} r_{L1} &= \omega_0 L / Q_{L1}, r_{Ls} = \omega_0 L_s / Q_{Ls}, r_{Lf} \\ &= \omega_0 L_f / Q_{Lf}, r_{LN} = \omega_0 L_N / Q_{LN} \\ Y_{L1} &= 1 / (j\omega_0 L_1 + r_{L1}), Y_{Ls} = 1 / (j\omega_0 L_s + r_{Ls}), \\ Y_{Lf} &= 1 / (j\omega_0 L_f + r_{Lf}) \\ Y_{ZLN} &= 1 / (j\omega_0 L_N + r_{LN} + Z_{L,N}), Y_{ZLs} \\ &= 1 / (j\omega_0 L_s + r_{Ls} + Z_{L,m}) \\ r_{C3} &= 1 / (\omega_0 C_3 Q_{C3}), Y_{C3} = 1 / [1 / (j\omega_0 C_3) + r_{C3}] \\ r_{CM} &= 1 / (\omega_0 C_M Q_{CM}), Y_{CM} \\ &= 1 / [1 / (j\omega_0 C_M) + r_{CM}] \\ r_{C1} &= 1 / [\omega_0 (C_1 - C_M) Q_{C1}], Y_{C1} \\ &= 1 / [1 / (j\omega_0 (C_1 - C_M)) + r_{C1}] \\ r_{C2} &= 1 / [\omega_0 (C_2 - C_M) Q_{C2}], Y_{C2} \\ &= 1 / [1 / (j\omega_0 (C_2 - C_M)) + r_{C2}] \end{aligned} \right. \quad (15)$$

where  $r_{L1}$ ,  $r_{Ls}$ ,  $r_{Lf}$ ,  $r_{LN}$ ,  $r_{C3}$ ,  $r_{CM}$ ,  $r_{C1}$ , and  $r_{C2}$  are the parasitic resistances of  $L_1$ ,  $L_s$ ,  $L_f$ ,  $L_N$ ,  $C_3$ ,  $C_M$ ,  $C_1-C_M$ , and  $C_2-C_M$ , respectively.  $Y_{L1}$ ,  $Y_{Ls}$ ,  $Y_{Lf}$ ,  $Y_{C3}$ ,  $Y_{CM}$ ,  $Y_{C1}$ , and  $Y_{C2}$  are the admittance of  $L_1$ ,  $L_s$ ,  $L_f$ ,  $C_3$ ,  $C_M$ ,  $C_1-C_M$ , and  $C_2-C_M$ , respectively.  $Y_{ZLN}$  is the admittance of the last load branch.  $Y_{ZLs}$  is the admittance of the rest of the load branches. Applying the node voltage method to Fig. 9, the following equation can be obtained as:

$$\begin{bmatrix} G_1 & B_1 & O_{2 \times 3} & O_{2 \times 3} & \dots & O_{2 \times 3} & O_{2 \times 3} \\ C_1 & G_2 & B_2 & O_{3 \times 3} & \dots & O_{3 \times 3} & O_{3 \times 3} \\ O_{3 \times 2} & C_2 & G_3 & B_3 & \dots & O_{3 \times 3} & O_{3 \times 3} \\ \dots & \dots & \dots & \dots & \dots & \dots & \dots \\ O_{3 \times 2} & O_{3 \times 3} & O_{3 \times 3} & O_{3 \times 3} & \dots & G_{N-1} & B_{N-1} \\ O_{3 \times 2} & O_{3 \times 3} & O_{3 \times 3} & O_{3 \times 3} & \dots & C_{N-1} & G_N \end{bmatrix} \begin{bmatrix} V_{p1} \\ V_{p2} \\ V_{p3} \\ \dots \\ V_{p(N-1)} \\ V_{pN} \end{bmatrix} = \begin{bmatrix} I \\ O_{3 \times 1} \\ O_{3 \times 1} \\ \dots \\ O_{3 \times 1} \\ O_{3 \times 1} \end{bmatrix} \quad (16)$$

where  $G_m$ ,  $B_m$ ,  $C_m$ ,  $V_{pm}$ , and  $I$  are as expressed as (17)–(21), respectively.  $O_{p \times q}$  represents the zero matrices with  $p$  rows and  $q$  columns

$$B_m = \begin{cases} [000; -Y_{ZLs}00] & m = 1 \\ [000; 000; -Y_{ZLs}00] & m = 2, 3, \dots, N-1 \end{cases} \quad (18)$$

$$\mathbf{C}_m = \begin{cases} [0 - Y_{ZLs}; 00; 00] & m = 1 \\ [00 - Y_{ZLs}; 000; 000] & m = 2, 3, \dots, N - 1 \end{cases} \quad (19)$$

$$\mathbf{V}_{pm} = \begin{cases} [\mathbf{V}_{P(3(m-1)+1)} \ \mathbf{V}_{P(3(m-1)+2)}]^\top & m = 1 \\ [\mathbf{V}_{P(3(m-1))} \ \mathbf{V}_{P(3(m-1)+1)} \ \mathbf{V}_{P(3(m-1)+2)}]^\top & m = 2, 3, \dots, N \end{cases} \quad (20)$$

$$\mathbf{I} = [-Y_{L1} \mathbf{V}_{in1} \ 0]^\top \quad (21)$$

where  $\mathbf{V}_{P1}$ ,  $\mathbf{V}_{P2}$ , ..., and  $\mathbf{V}_{PN}$  represent the node voltages and can be obtained by solving (16).  $\mathbf{I}_{L1}$ ,  $\mathbf{I}_{Lf, m}$  ( $m = 2, 3, \dots, N$ ),  $\mathbf{I}_{CM}$ ,  $\mathbf{I}_{C1, m}$ ,  $\mathbf{I}_{C2, m}$ ,  $\mathbf{I}_{C3, m}$ , and  $\mathbf{I}_{ZL, m}$  ( $m = 1, 2, \dots, N$ ) are the currents flowing through  $L_1$ ,  $L_{f, m}$ ,  $C_M$ ,  $C_{s, 2m-1}$ - $C_M$ ,  $C_{s, 2m}$ - $C_M$ ,  $C_3$ ,  $m$ , and  $Z_L$ ,  $m$  ( $m = 1, 2, \dots, N$ ), respectively. The directions of all currents are defined in Fig. 9. Applying Ohm's law, all currents can be calculated as (22).

To facilitate the comparisons of load output current variations, the normalized load output current and load power are obtained with their base values  $I_b$  and  $P_b$ , which can be calculated as

$$Z_b = 1 / [\omega C_M (1/k^2 - 1)], \quad I_b = V_{in1} / Z_b, \quad P_b = I_b^2 Z_b \quad (23)$$

where  $R_b$  is obtained by dividing  $V_{AmBm}$  by  $I_{ZL, m}$  ( $m = 1, 2, \dots, N$ ) according to (12). Assuming that the load current drop is small and all load currents are nearly equal to  $I_b$ , the  $m$ th load power  $P_{ZL, m}$  can be normalized by its base value  $P_b$  and the normalized load power  $P_{nom}$  can be derived as

$$P_{nom} = P_{ZL, m} / P_b = (I_{ZL, m}^2 Z_{L, m}) / (I_b^2 Z_b) \approx Z_L / Z_b. \quad (24)$$

To simplify the system analysis, the load impedance  $Z_L, m$  is regarded as resistive when analyzing the influence of parasitic resistances on load currents and system efficiency. Usually, the quality factors of all components in Fig. 9 are different. However, to simplify the analysis of the load currents and efficiency, the quality factors of all components are assumed the same as  $Q$ . Such assumptions will not affect the generality of conclusions, because only the specific values are different. Furthermore,

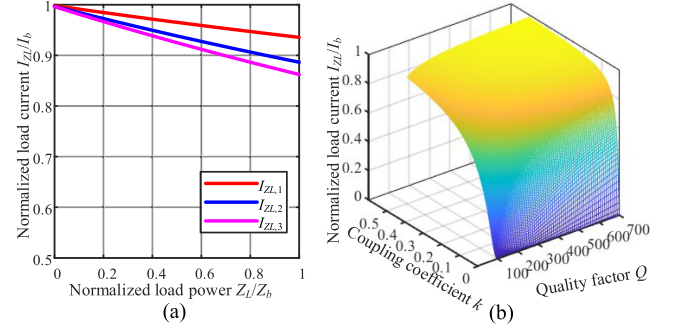


Fig. 11. Load current analysis. (a) Normalized load current variations versus the normalized load power ( $k = 0.15$  and  $Q = 500$ ). (b) Third load current variations with different coupling coefficients and quality factors ( $N = 3$  and  $Z_b/Z_L = 0.6$ ).

all load resistances are identical and change simultaneously in the following analysis of load current and system efficiency. Fig. 11(a) shows the normalized load current variations versus the normalized load power, which indicates the load currents decrease gradually as the load power increases. The further the distance between the load and Relay #0, the faster the load current drops. Thus, the last load current can be regarded as an evaluation criterion for the CC characteristic of the proposed system. Fig. 11(b) shows the third normalized load current variations with different coupling coefficients and quality factors. It should be noted that the third load current drop decreases with the increase of coupling coefficient and quality factor. Thus, a higher coupling coefficient or a higher quality factor is beneficial to obtain a better constant load currents characteristic.

The load output power  $P_{o, m}$  ( $m = 1, 2, \dots, N$ ) in each transmitter–receiver pair can be calculated as

$$P_{o, m} = I_{ZL, m}^2 Z_{L, m}. \quad (25)$$

The input power  $P_{in, m}$  ( $m = 1, 2, \dots, N$ ) in each transmitter–receiver pair is, (26) shown at bottom of next page.

$$\mathbf{G}_m = \begin{cases} \begin{bmatrix} Y_{L1} + Y_{C1} + Y_{CM} & -Y_{CM} & & \\ -Y_{CM} & Y_{ZLs} + Y_{C2} + Y_{CM} & & \\ & & & \end{bmatrix} & m = 1 \\ \begin{bmatrix} Y_{RLs} + Y_{C3} + Y_{Lf} & -Y_{Lf} & 0 & \\ -Y_{Lf} & Y_{Lf} + Y_{C1} + Y_{CM} & -Y_{CM} & \\ 0 & -Y_{CM} & \begin{cases} Y_{CM} + Y_{C2} + Y_{ZLs} & (m = 2, \dots, N - 1) \\ Y_{CM} + Y_{C2} + Y_{ZLN} & (m = N) \end{cases} & \end{bmatrix} & m = 2, 3, \dots, N \end{cases} \quad (17)$$

$$\begin{cases} \mathbf{I}_{L1} = |(\mathbf{V}_{in1} - \mathbf{V}_{P(3(m-1)+1)}) \cdot Y_{L1}| & m = 1 \\ \mathbf{I}_{Lf, m} = |(\mathbf{V}_{P(3(m-1))} - \mathbf{V}_{P(3(m-1)+1)}) \cdot Y_{Lf}| & m = 2, 3, \dots, N \\ \mathbf{I}_{CM, m} = |(\mathbf{V}_{P(3(m-1)+1)}) \cdot Y_{C1} - (\mathbf{V}_{P(3(m-1)+2)}) \cdot Y_{C2}| & m = 1, 2, \dots, N \\ \mathbf{I}_{C1, m} = |(\mathbf{V}_{P(3(m-1)+1)}) \cdot Y_{C1}|, \mathbf{I}_{C2, m} = |(\mathbf{V}_{P(3(m-1)+2)}) \cdot Y_{C2}| & m = 1, 2, \dots, N \\ \mathbf{I}_{C3, m} = |(\mathbf{V}_{P(3(m-1)+3)}) \cdot Y_{C3}| & m = 2, 3, \dots, N \\ \mathbf{I}_{ZL, m} = \begin{cases} |(\mathbf{V}_{P(3(m-1)+2)} - \mathbf{V}_{P(3(m-1)+3)}) \cdot Y_{ZLs}| & m = 1, 2, \dots, N - 1 \\ |(\mathbf{V}_{P(3(m-1)+2)}) \cdot Y_{ZL2}| & m = N \end{cases} \end{cases} \quad (22)$$

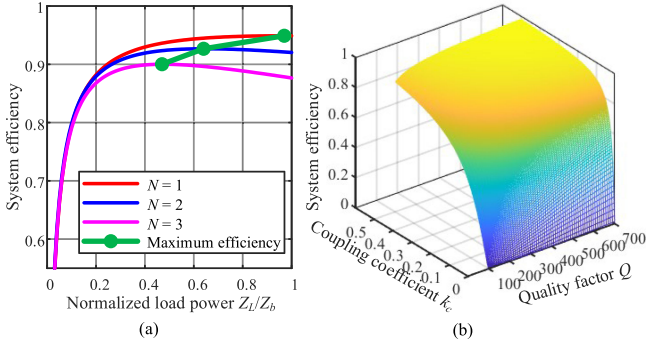


Fig. 12. System efficiency analysis. (a) System efficiency variation against the normalized load resistance. ( $N = 3$ ,  $k = 0.15$ , and  $Q = 500$ ). (b) Maximum achievable efficiency variations with different coupling coefficients and quality factors ( $N = 3$  and  $Z_b/Z_L = 0.6$ ).

Then, the efficiency  $\eta_N$  for  $N$  multiple loads can be derived as

$$\eta_N = \left( \sum_{m=1}^N P_{o,m} \right) / \left( \sum_{m=1}^N P_{in,m} \right). \quad (27)$$

Fig. 12(a) shows the system efficiency variation versus the normalized load power. It can be observed that as the number of loads increase, the system efficiency will decrease. As opposed to the one-load CPT system with only four plates where the maximum efficiency is achieved at  $Z_L/Z_b = 1$ , the optimal normalized load power for the multiload CPT relay system to achieve the maximum efficiency will decrease as the number of the load increases. This is because more power is consumed in the parasitic resistances of the compensation network and the capacitive coupling interface. Fig. 12(b) shows variations of the maximum achievable efficiency versus the coupling coefficient and quality factor in a three-load capacitive power relay system concluding that higher efficiency can be achieved with a higher coupling coefficient or a higher quality factor.

#### IV. EXPERIMENTS

##### A. Prototype Setup and Experimental Results

An experimental prototype consisting of one inverter and three loads is constructed, as shown in Fig. 13(a). Since the load currents are constant and the load power is nearly decoupled in the proposed system, the CC output characteristics will not be changed by the type of load. In this case, resistive loads are used to simplify the experimental verification. The SiC MOSFETs are adopted in the inverter to generate a source of 1.5 MHz ac for the compensation circuits. The input voltage  $V_{DC}$  of the inverter is 50 V. The dimensions of the multiload CPT relay system are consistent with the Maxwell simulation parameters

as shown in Section II-C. The coupling coefficient  $k$  of each transmitter–receiver pair is selected as 1.5. Adopting the derivation of compensation component parameters in Section III, the system specifications are given in Table II.  $L_{s,1,1}$  and  $L_{s,1,2}$  are slightly reduced by the same value to achieve zero-voltage switching (ZVS) for the MOSFETs. The compensation inductors are made of 660-strand Litz wire and are wound on the Polyvinyl Chloride (PVC) tube to eliminate the skin effect and magnetic losses. When the normalized load power is 0.186, the experimental waveforms are presented in Fig. 13(b) and (c). Referencing Fig. 13(b), the inverter output current lags the inverter output voltage, which indicates ZVS is achieved in this system. The first load output current lags the inverter output voltage by about  $90^\circ$ , and the adjacent load output currents are around  $180^\circ$  out of phase, which is consistent with the analysis in Section III.

Fig. 14(a) shows the load current variation versus the increasing load power. Normalized load current decreases gradually with the increase of the normalized load power, which is consistent with the analysis in Section III. It is worth noting that the system can still be regarded as multiple CC outputs although the slight load output current attenuation. The current decay can be decreased with a large  $k$  or  $Q$  as analyzed above. For some occasions with the requirement with different output currents, the dc/dc converter can be employed before each real load to regulate the output currents. This will not affect the validity of the proposed scheme because multiple loads are decoupled in this system. Therewithal, the proposed system can be easily modified to feed the loads with different currents by redesigning the compensation topology parameters according to (12) and (14). Even when the three load resistances are different, the load current variations are still within 3% as shown in Fig. 14(b), which indicates that the proposed multiload CPT relay system can retain the CC output characteristic with different load resistances.

The system efficiency variation versus the increasing load power is shown in Fig. 14(c). The optimal normalized load power is 0.403 to achieve the maximum efficiency of 86.1%. This efficiency is reasonable because of the inverter loss and the parasitic resistances in compensation topologies. Higher efficiency can be obtained with a large  $k$  or  $Q$  as analyzed in Section III. It is noticed that the efficiency can vary in a wide range from around 70% to 86.1% and the optimized system efficiency is related to the equivalent ac load impedance. In practical applications, dc–dc converter can be employed before each real load to dynamically change the equivalent ac load impedance so that the maximum efficiency tracking can be achieved. In this case, the system can work in a wide dynamic range.

Fig. 15 shows the transient behavior when the normalized load power  $Z_{L,1}/Z_b$ ,  $Z_{L,2}/Z_b$ , and  $Z_{L,3}/Z_b$  changes from 0.495

$$P_{in,m} = \begin{cases} I_{L1}^2 r_{L1} + I_{C1,m}^2 r_{C1} + I_{CM,m}^2 r_{CM} + I_{C2,m}^2 r_{C2} + I_{Ls,m}^2 r_{Ls} + P_{o,m} & m = 1 \\ I_{C3,m}^2 r_{C3} + I_{Lf,m}^2 r_{Lf} + I_{C1,m}^2 r_{C1} + I_{CM,m}^2 r_{CM} + I_{C2,m}^2 r_{C2} + I_{Ls,m}^2 r_{Ls} + P_{o,m} & m = 2, 3, \dots, N-1 \\ I_{C3,m}^2 r_{C3} + I_{Lf,m}^2 r_{Lf} + I_{C1,m}^2 r_{C1} + I_{CM,m}^2 r_{CM} + I_{C2,m}^2 r_{C2} + I_{LN}^2 r_{L2} + P_{o,m} & m = N \end{cases} \quad (26)$$

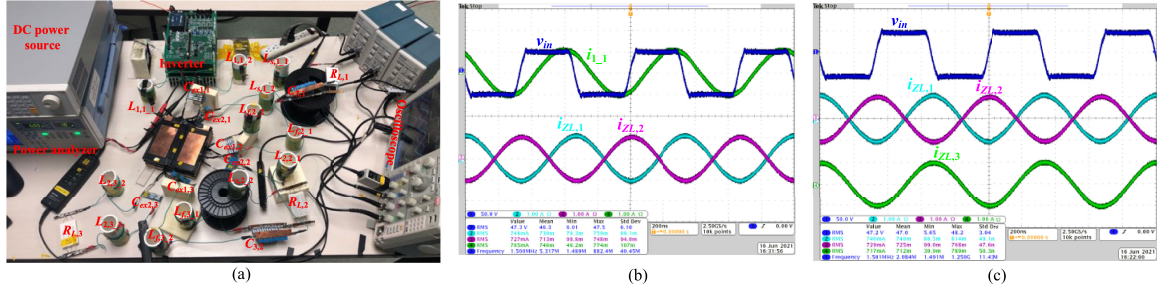


Fig. 13. Experimental setup and waveforms. (a) Experimental setup. (b) Experimental waveforms of inverter output voltage, current, and second and third load output currents. (c) Experiment waveforms of inverter output voltage and three load output currents.

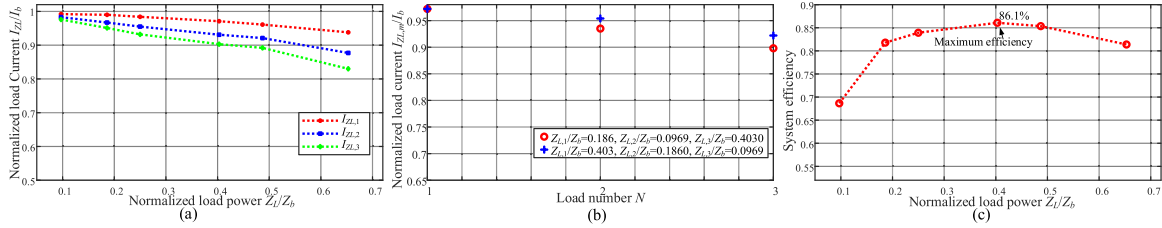


Fig. 14. Experimental results. (a) Load current variation versus the increasing normalized load power. (b) Load current variations with different normalized load powers. (c) System efficiency variation versus the increasing normalized load power.

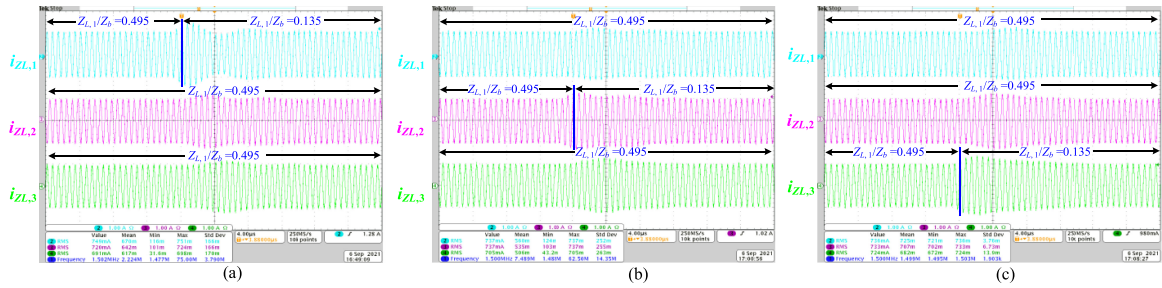


Fig. 15. Experimental results for transient behavior when the normalized load power changes from 0.495 to 0.135. (a)  $Z_{L,1}/Z_b$  changes and the other two loads remain unchanged. (b)  $Z_{L,2}/Z_b$  changes and the other two loads remain unchanged. (c)  $Z_{L,3}/Z_b$  changes and the other two loads remain unchanged.

to 0.135, respectively. As can be seen from Fig. 15(a), when  $Z_{L,1}$  changes while the other two loads remain unchanged,  $I_{ZL,1}$  immediately changes and the other two load currents  $I_{ZL,2}$  and  $I_{ZL,3}$  also change accordingly, but the starting instants that  $I_{ZL,2}$  and  $I_{ZL,3}$  change are slightly later than  $I_{ZL,1}$  and the degree of change is also less than  $I_{ZL,1}$ . Then after around  $8\mu s$ , the three load currents will stabilize again. In Fig. 15(b), only  $Z_{L,2}/Z_b$  changes to 0.135 while the other two loads remain unchanged. In Fig. 15(c), only  $Z_{L,3}/Z_b$  changes to 0.135 while the other two loads remain unchanged. It can be observed from Fig. 15(b) and (c) that the transient behavior is similar to that in Fig. 15(a). The above experimental waveforms indicate that when one load changes, the current flowing through the other two loads will also change subsequently. Then after a while, the output currents will stabilize at around the original value. Hence, the phenomena shown above prove that the proposed system renders good decoupling performance when the load changes.

Due to the parameter tolerance of devices, temperature rise and aging of the circuit components in practical applications, the

system performance will inevitably deviate from the nominal value. To maintain the normal operation of the system, the compensation capacitors and inductors can be replaced with variable switch-controlled capacitors or variable inductors [23], [24]. In the future, a control algorithm and tuning methods of  $LC$  components will be studied to obtain resonance conditions. The power density of the system can be further increased by increasing the switching frequency or dc input voltage of the inverter. In the future, compensation topology optimization will be studied to increase the power density. The power level of the proposed scheme can be improved by increasing the input voltage and the capacitive coupler area or decreasing the external capacitances according to (12) and (25).

### B. Electromagnetic Interference (EMI)

In the CPT system, the energy is transferred with the assistance of an electric field, which has the property of starting on the positive plate and ending on the negative plate [25]. Hence, the electric field contained in the capacitive coupler is the main

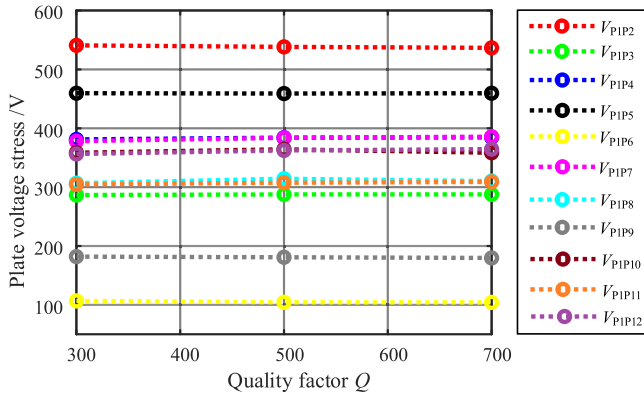


Fig. 16. Voltage stress across the capacitive coupler with different quality factors of the compensation components.

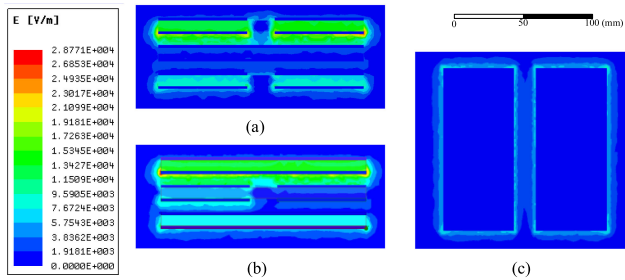


Fig. 17. Electric field intensity around the capacitive coupler. (a) Frontal plane. (b) Profile plane. (c) Top view.

TABLE III

COMPARISON OF THE MULTILOAD CPT SYSTEM IN [13] AND [15] AND THIS ARTICLE

Proposed in	[13]	[15]	This work
Number of loads	3	3	3
Efficiency	79% (DC-DC)	83.6% (DC-DC)	86.1% (DC-AC)
Power level	260W	15W	37W
Frequency	500kHz	10MHz	1.5MHz
Dielectric material	antistatic plastics	glass	Aluminum ceramic
Dielectric gap	0.2mm	1mm	8mm
Mutual capacitance $C_M$	15.6nF	370pF	39pF
Analysis of the coupling between receivers	No	No	Yes

cause of the EMI. The electric field intensity in the capacitive coupler is not only related to the size, but also related to the voltage applied to the plate [8]. The parasitic resistances in the compensation network have a very small effect on the voltage stress on the plate, as shown in Fig. 16. When the proposed system operates at maximum efficiency, the electric field intensity around the plates is simulated by the Ansys/Maxwell software, as shown in Fig. 17. It can be seen that there is no electric field if the distance is 13 mm away from the system.

### C. Comparison to Other Works

The comparison of the multiload CPT system in [13] and [15] and the work in this article is given in Table III. The selection

criteria for the above works are that they all power multiple loads simultaneously and a dielectric material is inserted between each transmitter–receiver pair. Furthermore, they all are experimentally verified. It can be seen that this article can achieve a high efficiency at a power level of 37 W with a lower mutual capacitance. Neither of the compared works has discussed how to eliminate the coupling between different receivers, however, in this article, the coupling between receivers is nearly zero by placing capacitive plates perpendicularly.

## V. CONCLUSION

A novel multiload CPT system with multiple relays has been proposed in this article, which can be used to charge batteries in series and powering multiple light emitting diodes. The relay is designed to power each load, where transmitting plates are placed perpendicularly to receiving plates with the assistance of the split-based compensation circuit to eliminate electric coupling. A general mathematic model of the capacitive coupler structure is provided when considering all coupling capacitances. The  $L$  and  $LCL$  compensation network with the corresponding resonant condition is utilized to obtain multiple load-independent CC outputs when neglecting parasitic resistances. The influence of the parasitic resistances on load currents and system efficiency are also presented, which indicates that a higher coupling coefficient or a higher quality factor is beneficial for the minimum load current drop and maximum efficiency. Finally, a three-load experimental prototype is constructed and the experimental results show that the system can achieve the maximum efficiency of 86.1%. Future research will focus on compensation topology optimization and the control algorithm for efficiency optimization.

## REFERENCES

- [1] J. Dai and D. C. Ludois, "A survey of wireless power transfer and a critical comparison of inductive and capacitive coupling for small gap applications," *IEEE Trans. Power Electron.*, vol. 30, no. 11, pp. 6017–6029, Nov. 2015.
- [2] Z. Zhang, H. Pang, A. Georgiadis, and C. Cecati, "Wireless power transfer—An overview," *IEEE Trans. Ind. Electron.*, vol. 66, no. 2, pp. 1044–1058, Feb. 2019.
- [3] V.-B. Vu, M. Dahidah, V. Pickert, and V.-T. Phan, "An improved LCL-L compensation topology for capacitive power transfer in electric vehicle charging," *IEEE Access*, vol. 8, pp. 27757–27768, 2020.
- [4] F. Lu, H. Zhang, H. Hofmann, and C. C. Mi, "A double-sided LC-compensation circuit for loosely coupled capacitive power transfer," *IEEE Trans. Power Electron.*, vol. 33, no. 2, pp. 1633–1643, Feb. 2018.
- [5] J. Lian and X. Qu, "Design of a double-sided LC compensated capacitive power transfer system with capacitor voltage stress optimization," *IEEE Trans. Circuits Syst. II, Express Briefs*, vol. 67, no. 4, pp. 715–719, Apr. 2020.
- [6] H. Zhang, F. Lu, H. Hofmann, W. Liu, and C. Mi, "A 4-plate compact capacitive coupler design and LCL-compensated topology for capacitive power transfer in electric vehicle charging applications," *IEEE Trans. Power Electron.*, vol. 31, no. 12, pp. 8541–8851, Dec. 2016.
- [7] F. Lu, H. Zhang, H. Hofmann, and C. Mi, "A double-sided LCLC-compensated capacitive power transfer system for electric vehicle charging," *IEEE Trans. Power Electron.*, vol. 30, no. 11, pp. 6011–6014, Nov. 2015.
- [8] J. Lian, X. Qu, X. Chen, and C. C. Mi, "Design of a double-sided LCLC compensated capacitive power transfer system with predesigned coupler plate voltage stresses," *IEEE J. Emerg. Sel. Topics Power Electron.*, to be published, doi: 10.1109/JESTPE.2020.3030657.

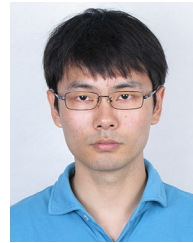
- [9] R. Mai, B. Luo, Y. Chen, and Z. He, "Double-sided CL compensation topology based component voltage stress optimisation method for capacitive power transfer charging system," *IET Power Electron.*, vol. 11, no. 7, pp. 1153–1160, 2018.
- [10] D. Jiejian and D. C. Ludois, "Single active switch power electronics for kilowatt scale capacitive power transfer," *IEEE J. Emerg. Sel. Topics Power Electron.*, vol. 3, no. 1, pp. 315–323, Jan. 2015.
- [11] M. Liu, M. Fu, Y. Wang, and C. Ma, "Battery cell equalization via megahertz multiple-receiver wireless power transfer," *IEEE Trans. Power Electron.*, vol. 33, no. 5, pp. 4135–4144, May 2018.
- [12] Y. Li *et al.*, "Analysis, design, and experimental verification of a mixed high-order compensations-based WPT system with constant current outputs for driving multistring leds," *IEEE Trans. Ind. Electron.*, vol. 67, no. 1, pp. 203–213, Jan. 2020.
- [13] Y.-G. Su, S.-Y. Xie, A. P. Hu, C.-S. Tang, W. Zhou, and L. Huang, "Capacitive power system with a mixed-resonant topology for constant-current multiple-pickup applications," *IEEE Trans. Power Electron.*, vol. 32, no. 11, pp. 8778–8786, Nov. 2017.
- [14] B. Minnaert, F. Mastri, A. Costanzo, M. Mongiardo, and N. Stevens, "Optimizing the power output for a capacitive wireless power transfer system with  $n$  receivers," in *Proc. IEEE Wireless Power Transf. Conf.*, 2019, pp. 351–354.
- [15] M. B. Lillholm, Y. Dou, X. Chen, and Z. Zhang, "Analysis and design of 10 MHz capacitive power transfer with multiple independent outputs for low power portable devices," *IEEE J. Emerg. Sel. Topics Power Electron.*, to be published, doi: [10.1109/JESTPE.2020.3035493](https://doi.org/10.1109/JESTPE.2020.3035493).
- [16] V. Vu *et al.*, "A multi-output capacitive charger for electric vehicles," in *Proc. IEEE 26th Intel. Symp. Ind. Electron.*, 2017, pp. 565–569.
- [17] A. Kumar, S. Pervaiz, C. Chieh-Kai, S. Korhummel, Z. Popovic, and K. K. Afridi, "Investigation of power transfer density enhancement in large air-gap capacitive wireless power transfer systems," in *Proc. IEEE Wireless Power Transf. Conf.*, 2015, pp. 1–4.
- [18] C. Cheng *et al.*, "Load-independent wireless power transfer system for multiple loads over a long distance," *IEEE Trans. Power Electron.*, vol. 34, no. 9, pp. 9279–9288, Sep. 2019.
- [19] C. Cheng *et al.*, "A load-independent LCC-compensated wireless power transfer system for multiple loads with a compact coupler design," *IEEE Trans. Ind. Electron.*, vol. 67, no. 6, pp. 4507–4515, Jun. 2020.
- [20] H. Zhang, F. Lu, H. Hofmann, W. Liu, and C. C. Mi, "An LC-compensated electric field repeater for long-distance capacitive power transfer," *IEEE Trans. Ind. Appl.*, vol. 53, no. 5, pp. 4914–4922, May 2017.
- [21] W. Zhou, L. Huang, B. Luo, R. Mai, Z. He, and A. P. Hu, "A general mutual coupling model of mimo capacitive coupling interface with arbitrary number of ports," *IEEE Trans. Power Electron.*, vol. 36, no. 6, pp. 6163–6167, Jun. 2021.
- [22] Y. Wu, Q. Chen, X. Ren, and Z. Zhang, "Efficiency optimization based parameter design method for the capacitive power transfer system," *IEEE Trans. Power Electron.*, vol. 36, no. 8, pp. 8774–8785, Aug. 2021.
- [23] Z. Huang, C.-S. Lam, P.-I. Mak, R. P. Martins, S. C. Wong, and C. K. Tse, "A single-stage inductive-power-transfer converter for constant-power and maximum-efficiency battery charging," *IEEE Trans. Power Electron.*, vol. 35, no. 9, pp. 8973–8984, Sep. 2020.
- [24] X. Wang, J. Xu, S. Lu, S. Ren, M. Leng, and H. Ma, "Single-receiver multi-output inductive power transfer system with independent regulation and unity power factor," *IEEE Trans. Power Electron.*, vol. 37, no. 1, pp. 1159–1171, Jan. 2022.
- [25] D. Rozario, N. A. Azeez, and S. S. Williamson, "A modified resonant converter for wireless capacitive power transfer systems used in battery charging applications," in *Proc. IEEE Transp. Electrific. Conf. Expo.*, 2016, pp. 1–6.



of switching converters.

**Ting Chen** received the B.S. and M.S. degrees in 2015 and 2017, respectively, from the China University of Mining and Technology, Beijing, China, where she is currently working toward the Ph.D. degree.

From November 2019 to November 2021, she was a joint Ph.D. student funded by the China Scholarship Council with the Department of Electrical and Computer Engineering, San Diego State University, San Diego, CA, USA. Her current research interests include wireless power transfer technologies, high power multilevel converters, modeling, and control



**Chenwen Cheng** received the B.S. and Ph.D. degrees in electrical engineering from Zhejiang University, Hangzhou, China, in 2012 and 2017, respectively.

From 2018 to 2021, he was a Postdoctoral Researcher with San Diego State University, San Diego, CA, USA. He is currently with Southeast University, Nanjing, China. His research interests include the motor control, renewable power generation, and wireless power transfer technologies.



power electronics equipment.

**Hong Cheng** received the B.S. degree from Beihang University, Beijing, China, in 1988, and the Ph.D. degree from the China University of Mining and Technology, Beijing, in 1993, both in electrical engineering.

She is currently a Professor of power electronics with the School of Mechanical Electronic and Information Engineering, China University of Mining and Technology. Her current research interests include high power multilevel converters, modeling and control of switching converters, and fault diagnosis of



of power electronics with the School of Mechanical Electronic and Information Engineering, China University of Mining and Technology. His current research interests include high power multilevel converters, high-frequency soft-switching converters, and power electronics in smart grid.

**Cong Wang** was born in Beijing, China, in 1955. He received the B.S. degree from the Taiyuan University of Technology, Taiyuan, China, in 1982, and the M.S. and Ph.D. degrees from the China University of Mining and Technology, Beijing, China, in 1984 and 2005, respectively, all in electrical engineering.

From 1990 to 1991, he was a Visiting Scholar with the University of Bristol, Bristol, U.K. From 2002 to 2003, he was a Senior Visiting Scholar and a Visiting Professor with the University of Tennessee, Knoxville, TN, USA. He is currently a Professor



Electric Company, Peterborough, ON, Canada, from 2000 to 2001. His research interests include electric drives, power electronics, electric machines, renewable-energy systems, electrical and hybrid vehicles, battery management systems, and wireless power transfer.

**Chunting Chris Mi** (Fellow, IEEE) received the B.S.E.E. and M.S.E.E. degrees from Northwestern Polytechnical University, Xi'an, China, and the Ph.D. degree from the University of Toronto, Toronto, ON, Canada, in 1985, 1988, and 2011, respectively, all in electrical engineering.

He is currently a Professor of electrical and computer engineering, San Diego State University, San Diego, CA, USA. Previously, he was a Faculty member with the University of Michigan, Dearborn, MI, USA, from 2001 to 2015. He was with General

Electric Company, Peterborough, ON, Canada, from 2000 to 2001. His research interests include electric drives, power electronics, electric machines, renewable-energy systems, electrical and hybrid vehicles, battery management systems, and wireless power transfer.

Dr. Mi is the recipient of "Distinguished Teaching Award" and "Distinguished Research Award" from the University of Michigan Dearborn, 2007 IEEE Region 4 "Outstanding Engineer Award," "IEEE Southeastern Michigan Section Outstanding Professional Award," "SAE Environmental Excellence in Transportation (E2T) Award," IEEE Transactions on Power Electronics Best Paper Awards and Prize Letter Award, as well as the IEEE Power Electronics Emerging Technology Award. He was the Chair (2008–2009) and the Vice Chair (2006–2007) of the IEEE Southeastern Michigan Section. He was an Area Editor for the IEEE TRANSACTIONS ON VEHICULAR TECHNOLOGY, an Associate Editor for the IEEE TRANSACTIONS ON POWER ELECTRONICS, and an Associate Editor for the IEEE TRANSACTIONS ON INDUSTRY APPLICATIONS. He is the Guest Editor of the recent special of the Proceedings of the IEEE. He is a Fellow of the SAE.